Cambridge Centre for Computational Chemical Engineering

Studying the Influence of Direct Injection on PCCI Combustion and Emissions at Engine Idle Condition Using Two dimensional CFD and Stochastic Reactor Model

Li Cao, Haiyun Su, Sebastian Mosbach, Markus Kraft [1] , Amit Bhave [1,2]

released: 19 January 2008

[1] Department of Chemical Engineering
University of Cambridge
New Museums Site
Pembroke Street
Cambridge, CB2 3RA
UK
E-mail: mk306@cam.ac.uk

[2] Reaction Engineering Solutions Ltd.
William Gates Building
JJ Thompson Avenue
Cambridge, CB3 0FD
UK
E-mail: ab349@cam.ac.uk

Preprint No. 54

c4e

Abstract

A detailed chemical model was implemented in the KIVA–3V two dimensional CFD code to investigate the effects of the spray cone angle and injection timing on the PCCI combustion process and emissions in an optical research diesel engine. A detailed chemical model for Primary Reference Fuel (PRF) consisting of 157 species and 1552 reactions was used to simulate diesel fuel chemistry. The model validation shows good agreement between the predicted and measured pressure and emissions data in the selected cases with various spray angles and injection timings. If the injection is retarded to -50° ATDC, the spray impingement at the edge of the piston corner with 100° injection angle was shown to enhance the mixing of air and fuel. The minimum fuel loss and more widely distributed fuel vapour contribute to improving combustion efficiency and lowering uHC and CO emissions in the engine idle condition. Finally, the coupling of CFD and multi–zone Stochastic Reactor Model (SRM) was demonstrated to show improvement in CO and uHC emissions prediction.

1

Contents

1 Introduction

Improving fuel economy and reducing emissions are two major challenges faced by the automotive industry. Over the recent years, Homogeneous Charge Compression Ignition (HCCI) or Premixed Charge Compression Ignition (PCCI) combustion, has been receiving increased attention due to its potential for simultaneously reducing fuel consumption and NO_x emissions in a gasoline Spark Ignition (SI) engine, and its capability to remove soot and NO_x emissions from a Compression Ignition Direct Injection (CIDI) diesel engine. PCCI combustion is achieved by controlling the temperature, pressure, and composition of the fuel and air mixture, so that it spontaneously ignites in an engine. This unique characteristic of PCCI allows the combustion of very lean or diluted mixtures using internal or external EGR, resulting in low temperatures that dramatically reduce the engine-out NO_x emissions. Similar to an SI engine, the combustible charge is well premixed and hence it minimizes particulate emissions.

As the concept of PCCI involves the premixed combustion of a highly diluted mixture, the combustion process is primarily controlled by the chemical kinetics. Thus, the control of ignition timing and burning rate in PCCI combustion is fundamentally more challenging than in conventional diesel engine, which is governed mainly by the physical processes such as fuel injection rate and fuel-air mixing. In addition, the narrow operation range for PCCI combustion is constrained by the upper knocking and lower misfire limits. Many researchers have explored various control strategies to overcome the aforementioned technical obstacles. It has been demonstrated that PCCI combustion can be promoted by increasing compression ratio [4], heating of intake air and/or fuel [6, 13], utilizing the internal or external EGR [8, 13] and using dual fuels [10, 21].

Preliminary research indicates that the operation range can be extended significantly by controlling charge stratification. Perhaps the most straightforward way to control the charge stratification in a PCCI engine is to inject fuel directly into the cylinder. In order to ensure sufficient time for mixing, the fuel injection timing is much advanced compared to the conventional CIDI diesel engine. On account of the low volatility of diesel fuel, the early injection with the conventional wide spray angle injector in low ambient gas density condition can result in very serious spray impingement and wall wetting, contributing to a dramatic increase in emissions and incomplete combustion or misfire in the low load range. Using a narrow spray angle to contain the spray in the bowl [19] or multiple injections [11, 13, 16] could be possible solutions.

A variety of computational modelling approaches have been applied to investigate PCCI combustion. Multi-zone models are the simplest methods that have been applied to PCCI combustion. The simplified fluid dynamics permits relatively large kinetic mechanisms to be included. These models can be divided into two methods: (1) Coupled CFD Multi–zone chemistry solver [1, 3, 5], and (2) Direct integration with detailed chemistry [12]. The first method essentially decouples the numerical solution of the chemistry from that of the fluid dynamics. The computational domain in the CFD code is divided into a lim-

ited number of zones (usually < 100), each characterized by temperature and equivalence ratio. In contrast, the direct integration with detailed chemistry involves the use of detailed kinetics to solve the chemistry within each computational cell in the CFD domain. Both methods rely on the assumption that the variations in the scalar variables (temperature and equivalence ratio) are negligible within each zone or computational cell. Since the validity of this assumption relies on the size of the zones, the direct integration approach with detailed chemistry gives a better prediction than multi–zone model in the presence of significant stratification [12]. However, a more direct and better representation of the complex interactions occurring in small length scales between turbulence and kinetics can be achieved by implementing a more advanced turbulent combustion model. Zhang et. al. [22] used a joint PDF containing 40 chemical species and mixture enthalpy to model HCCI combustion. Their results demonstrate the importance of accounting for turbulence–chemistry interactions with increasing stratification. Unfortunately, the method becomes computationally expensive as the number of species in the reaction mechanism increases.

In the present paper, a detailed chemical mechanism comprising of 157 chemical species and 1552 reactions was incorporated within the KIVA 3V code. To maintain reasonable computational time of the kinetics based calculations, a 2D grid was employed to investigate the effect of the spray angle and injection timing on combustion characteristics, pressure and engine-out emissions in an optical research diesel engine. In this study, the reaction rate is formulated to incorporate the effects of both chemical kinetics and turbulent mixing by using the characteristic timescale combustion model [12]. The uncertainties of reaction rate closure involved with this method are not within the scope of this paper and will be included in future work. Another motivation of this study is to extract the spatial distribution of fuel and the turbulent mixing time from CFD results to improve the PDF based Stochastic Reactor Model (SRM) [14], and enable cycle to cycle simulation with low computational costs while providing sufficiently reliable predictions of emissions.

This paper is structured as follows: in the next section, CFD–chemical kinetics combustion model and the Stochastic Reactor Model (SRM) are explained. This is followed by the description of the engine setup and model validation. In the next section, a parametric study of the influence of spray angle and injection timing on combustion characteristics and emissions is included. Finally, an improved emissions prediction achieved on account of the one–way coupling between multi–zone SRM model and CFD is demonstrated.

2   Modelling description

The CFD simulations were carried out by using the KIVA3V code [2], with improvements in turbulence, gas/wall heat transfer, spray breakup and combustion models. The RNG turbulence model was used for the engine flow simulation; the present wall heat

transfer model [7] uses a modified temperature wall function to account for density variations in the boundary layers; a hybrid breakup model, combining Kelvin–Helmholtz (KH) and Rayleigh–Taylor (RT) instability wave mechanisms, was applied to simulate high pressure cone spray atomization. The effects associated with spray/wall interactions including droplet splash and film spreading due to impingement forces were considered in a wall–film submodel [17]. The physical properties of tetradecane were used to simulate the physics of diesel fuel, while a detailed n–heptane reaction mechanism was used to simulate diesel fuel chemistry.

2.1   Spray breakup model

The fuel spray is modeled by assuming a liquid core emerging from the nozzle, which disintegrates very fast into droplets. The liquid jets are modeled as "blobs" with initial diameter equal to the nozzle size. The KH–RT hybrid breakup model is used for the primary and secondary atomization of the resulting droplets [18].

The Kelvin–Helmholtz model assumes that a parent parcel with radius, r , breaks up to form new droplets with radius, r_c , such that

$$r_c = B_0 \Lambda_{KH} \tag{1}$$

where Λ_{KH} is the wavelength corresponding to the KH wave with the maximum growth rate, Ω_{KH}, and B_0 is a constant equal to 0.61. The frequency of the fastest-growing wave and its corresponding wavelength are given by

$$\Omega_{KH} = \frac{0.34 + 0.38 We_g^{1.5}}{(1 + Z)(1 + 1.4T^{0.6})} \sqrt{\frac{\sigma}{\rho_f r^3}} \tag{2}$$

$$\Lambda_{KH} = \frac{9.02(1 + 0.45\sqrt{Z})(1 + 0.4T^{0.7})}{(1 + 0.865 We_g^{1.67})^{0.6}} \tag{3}$$

where the gas Weber number, $We_g = \frac{\rho_g U_r^2 r}{\sigma}$, the Ohnesorge number, $Z = \frac{\sqrt{We_l}}{Re_l}$, and the Taylor number, $T = Z\sqrt{We_g}$, U_r is the relative velocity between the liquid drop and the gas, σ is the surface tension, ρ_g and ρ_f are the gas and fuel densities, respectively.

During breakup, the parent parcel reduces in diameter due to the loss of mass. The rate of change of the radius of the parent parcel is calculated using

$$\frac{dr}{dt} = \frac{r - r_c}{\tau_{KH}} \tag{4}$$

where τ_{KH} is the breakup time defined by

$$\tau_{KH} = \frac{3.726 B_1 r}{\Omega_{KH} \Lambda_{KH}} \tag{5}$$

in this study, the constant B_1 is in the range of $10 \sim 60$.

The KH model is used to predict the initial breakup of the injected "blobs" or the intact liquid core. The Rayleigh–Taylor model is then used together with the KH model to predict the secondary breakup of the droplets. The RT model predicts instabilities on the surface of the drop that grow until a certain characteristic breakup time when the drop finally breaks up. The frequency of the fastest growing wave in the RT model is given by

$$\Omega_{RT} = \sqrt{\frac{2}{3\sqrt{3}\sigma} \frac{[-g_l(\rho_f - \rho_a)]^{\frac{3}{2}}}{\rho_f + \rho_a}} \tag{6}$$

where g_l is the acceleration of the droplet.

If the RT wave has been growing for a time greater than the breakup time, the drop is assumed to breakup. The radius of the new droplet is calculated using

$$r_c = \frac{\pi C_{RT}}{K_{RT}} \tag{7}$$

where the wave number, $K_{RT} = \sqrt{\frac{-g_l(\rho_f - \rho_a)}{3\sigma}}$, C_{RT} is a constant set equal to 0.2 in this study.

2.2 KIVA–chemical kinetics combustion model

The coupling between CFD and chemical kinetics is shown in Figure 1. An in–house chemistry package (SPROG) extracts the specific heat capacity ($C_{v,i}$), enthalpy (h_i) and molecular weight (mw_i) of each species, which are subsequently used in the CFD code, KIVA. The SPROG package is also used for interpreting the kinetics mechanism and obtaining the chemical source terms. The KIVA code provides the numerical solver (RADAU5) with the species mass fraction and temperature of each computational cell, and the chemical kinetics Ordinary Differential Equation (ODE) sets are then solved for every computational cell at each timestep. During the chemistry solution, the CFD timestep is taken as the integration time in the numerical solver to obtain new mixture conditions and energy release in each computational cell, which are then updated in the CFD code. The sub–grid interaction of turbulence and chemistry is considered by using the characteristics timescale concept [12], in which the reaction rate is mainly determined by a kinetic timescale and a turbulent timescale. This modelling work is a first step towards coupling of the Stochastic Reactor Model (SRM) with CFD, aiming at accounting for the interaction of chemical kinetics and turbulence, while reducing the computational cost simultaneously.

If the chemistry solutions were directly used in the KIVA code, the species conversion rates would be considered as kinetics controlled. However, the use of kinetics controlled

reaction rate usually results in too fast combustion rate [12]. This indicates that there may exist inevitable inhomogeneities in the mixture. Therefore, in the current model, a new reaction rate for each species is formulated to incorporate the effects of both chemical kinetics and turbulent mixing. The kinetic timescale is the time needed for a species to reach its equilibrium state under perfectly homogeneous conditions, while the turbulent timescale is the time of eddy breakup in order to mix the fuel, oxidizer, and hot combustion products. When the effect of sub–grid scale turbulence on the reaction rate is considered, the reaction rate is assumed to be mainly determined by a kinetic timescale and a turbulent timescale as below:

$$\omega_i = \frac{Y_i^* - Y_i}{\tau_{kin,i} + f\tau_{turb}} \tag{8}$$

where, for species i, Y_i and Y_i^* are the current and equilibrium concentrations respectively, $\tau_{kin,i}$ and τ_{turb} are the kinetic and turbulent timescales; the delay coefficient, $f = \frac{(1-e^{-r})}{0.632}$, here r is the ratio of the amount of products to that of total reactive species, indicating that the turbulence starts to have effects after the onset of ignition.

If turbulent effects on the reaction rate are ignored, Eq. (8) can be simplified to a kinetics controlled reaction rate,

$$\omega_{kin,i} = \frac{Y_i^* - Y_i}{\tau_{kin,i}} = \frac{\Delta Y_i}{dt} \tag{9}$$

where ΔY_i is the concentration change obtained by solving the chemical kinetics.

The kinetic time scale can be rewritten from Eq. (9),

$$\tau_{kin,i} = \frac{Y_i^* - Y_i}{\Delta Y_i} dt = \frac{Y_i^* - Y_i}{\tau_{kin,i}} = \frac{\Delta Y_i}{dt} \tag{10}$$

However, it is impractical to solve the equilibrium concentration and the kinetic timescale for each species in the detailed chemical kinetic mechanisms. Two assumptions are made to simplify this calculation process as formulated in ref.[12]. First, the kinetic timescale for all the species is assumed to be equal to that of the fuel. Second, the equilibrium concentration of the fuel is assumed to be zero, since the fuel is likely to react into intermediate species soon after the reaction has started. Therefore, the kinetic timescale and equilibrium concentration of each species can be derived as below:

$$\tau_{kin} = \left(\frac{-Y_f}{\Delta Y_f}\right) dt \tag{11}$$

$$Y_i^* - Y_i = \tau_{kin} \frac{\Delta Y_i}{dt} \tag{12}$$

By combining Eq. (8) and Eq. (12), an updated species at the current timestep, Y_i^{n+1}, can be obtained as

$$Y_i^{n+1} - Y_i^n = \omega_i dt = \frac{\tau_{kin}}{\tau_{kin} + f\tau_{turb}} \Delta Y_i \tag{13}$$

7

2.3 Stochastic reactor model (SRM)

The PDF–based Stochastic Reactor Model (SRM) is derived from the reduced PDF transport equation for scalars assuming statistical homogeneity and has been applied previously to HCCI engine simulation successfully [14, 15, 20]. The main feature of the SRM model is that it can account for scalar micro–mixing and fluctuations in quantities, which the multi–zone models cannot. The same chemical mechanism as that implemented in CFD was used. A Monte Carlo method with a second–order operator splitting technique is employed to solve the PDF transportation equation. For the description of turbulent mixing, the Euclidean Minimal Spanning Tree (EMST) model [15] was used, in which particles undergoing mixing are chosen based on proximity in composition space. A simplistic spray model was incorporated in the SRM to simulate early direct injection. Further details can be seen in reference [15].

3 Experimental setup and model validation

The engine used in this study was a single–cylinder, direct injection, 4–stroke optical diesel engine equipped with a common-rail fuel injection system [13]. The engine specifications are summarized in Table 1 and the geometry of the combustion chamber is shown in Figure 2. The fuel was injected using a 5 hole sac–type injector with various injection angles ($70° \sim 150°$). The intake air was preheated by an electric heater to achieve PCCI combustion. During the tests, in–cylinder pressure was recorded with a piezoelectric pressure transducer (KISTLER, 6052A) at every 0.16 Crank Angle Degree (CAD) and ensemble–averaged over 130 engine cycles. The apparent heat release rate was calculated from the averaged pressure data using the typical first law and perfect gas analysis [9]. The emissions measurement system (Horiba, MEXA 500D) was used to measure the concentrations of NO_x, uHC and CO. The detailed description of the experiment can be found in reference [13].

Table 1: *Engine specifications*

Engine	Single–cylinder, direct injection, four–valves,optical diesel engine
Bore×Stroke	$83 \times 92\,\text{mm}$
Displaced volume	$498\,\text{cm}^3$
Compression ratio	18.9
Fuel injection system	Bosch common rail
Injector	5 hole, Sac–type, nozzle diameter 0.168 mm
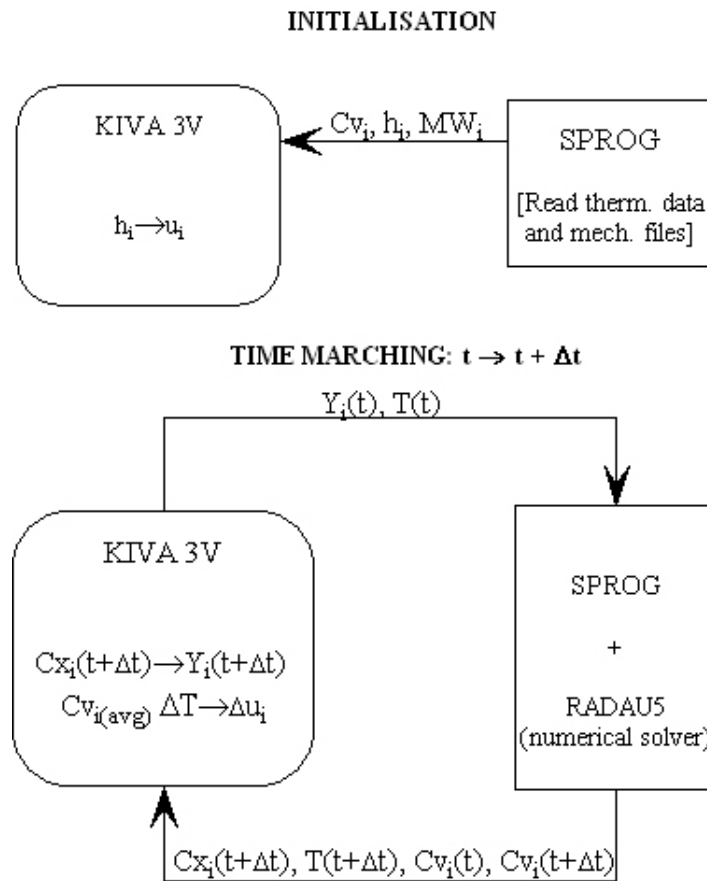
Figure 1: *Structure of coupling of CFD and chemical kinetics.*

Table 2: *Engine operating conditions*

Engine speed	800 rpm
Injection pressure	120 MPa
Injection timing	-200°, -100° and -50° ATDC
Injection angle	-70°, -100° and -150°
Injection duration	3°
Total amount of fuel	11.5 mm^3
Intake air temperature	433 K
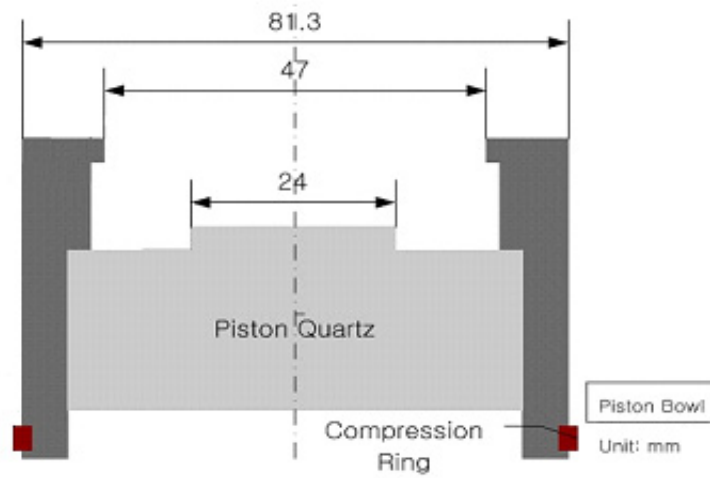
Figure 2: *The geometry of the combustion chamber.*

The engine operating conditions for this study are listed in Table 2. The engine was run at idle condition (800 rpm). Intake air was preheated to 433 K, so as to enhance the evaporation of diesel fuel and initiate PCCI combustion in the low load and idle conditions. The fuel quantity of 11.5 mm^3 was fixed for each injection. In order to systematically investigate the effect of injection parameters on PCCI combustion, the injection timings of the swept range vary from -200°, -100° and -50° ATDC, while the injection angles change from 70°, 100° and 150°.

Accurate modeling of spray characteristics is essential to better understand the fuel distribution and wall-impingement in the combustion chamber. Therefore, the spray model constants need to be tuned, before they are applied to PCCI combustion with early injection strategy. Figure 3 shows the measured radial penetration for the five–hole injector with 100° injection angle. The empirical constant B_1 in KH model and C_{RT} in RT model that control the secondary atomization rate were set to 30 and 0.2 respectively throughout this study. The qualitative comparison of spray penetration between the predicted and
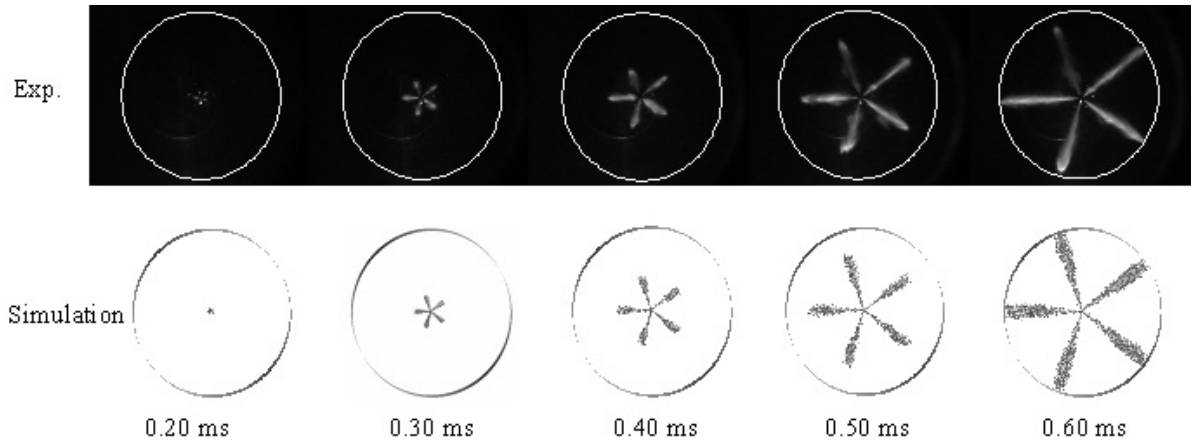
Figure 3: *Spray penetration comparison at several times after SOI (injection angle 100°)*
.

measured data is also included in Figure 3. The prediction captures the transient spray behavior well, as compared with the fuel spray observed in the experiment.

Due to the computational costs associated with accounting for the detailed reaction mechanism, the computations used 2D mesh (3200 grid cells at BDC) and started from IVC assuming a homogeneous distribution of temperature and mixture composition as the initial conditions. The temperatures of the cylinder wall, piston and cylinder head were set to 450, 500 and 500 K, respectively. Pressure profiles and apparent heat release rates were compared with the experimental results for the selected cases listed in Table 3. As shown in Figure 4, the simulation predictions are seen to agree reasonably well with the measured pressures. The detailed chemistry model is capable of reproducing the ignition delay, main apparent heat release rate and the peak pressure.

The predicted and measured pollutant emissions are compared for the selected cases as given in Table 3. The CO emission is slightly over-predicted, especially for the very early injection cases. This can perhaps be explained by the higher quantity of fuel vaporized and involved in low–temperature combustion in the simulation, (due to the over–predicted spray breakup process). It is a challenge to use the KH–RT hybrid breakup model for the early injection at low ambient gas density condition. However, the predictions capture the trends observed in the experimental results reasonably well.

11
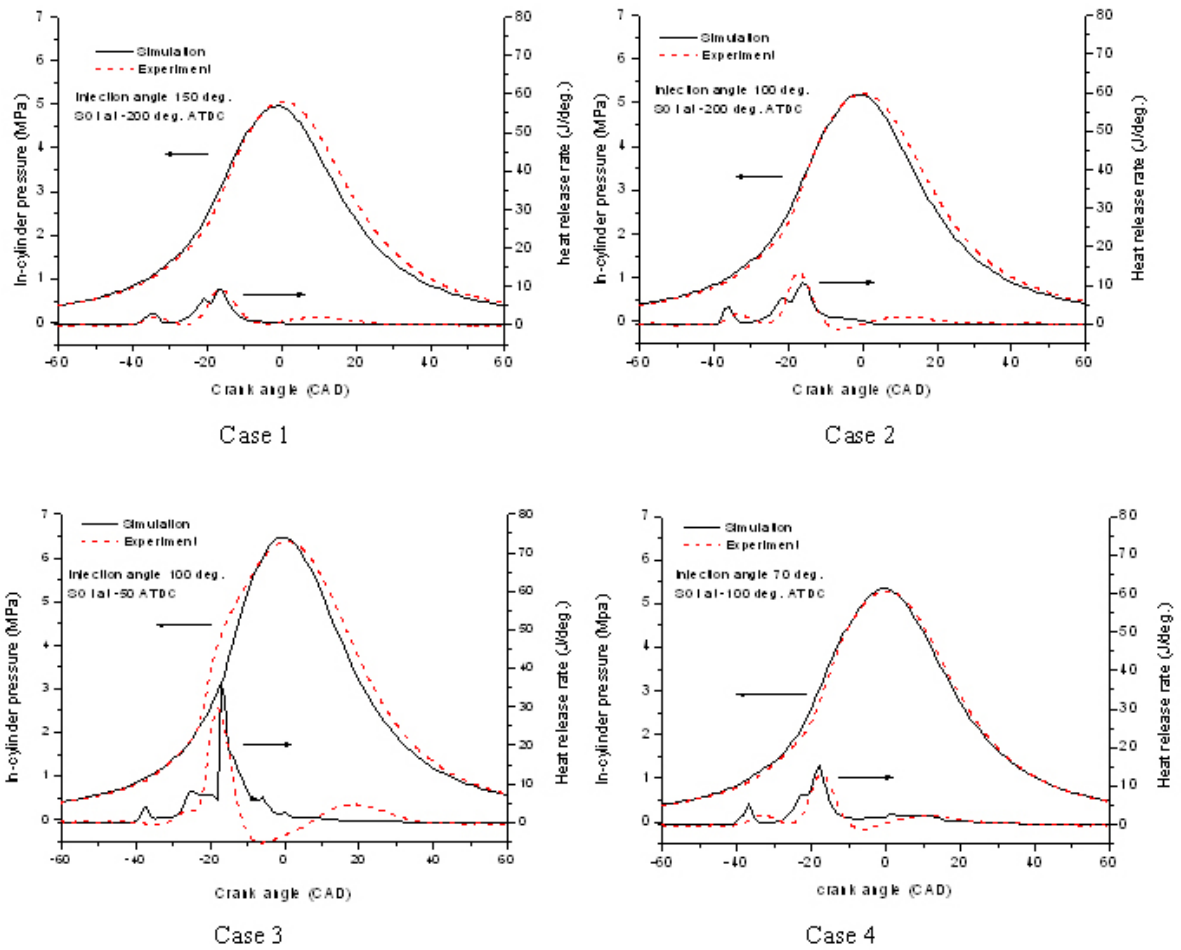
Figure 4: *Comparison between the predicted and measured pressure traces and heat release rates.*

Table 3: *Comparison between the predicted and measured engine–out emissions*

	Start of injection (ATDC)	Injection angle	NO_x (ppm)		CO (ppm)		uHC (ppm)	
			Sim.	Exp.	Sim.	Exp.	Sim.	Exp.
Case 1	-200°	150°	2.1E-4	4	8200	4878	6552	6213
Case 2	-200°	100°	4.1E-4	5	7043	3268	6157	4153
Case 3	-50°	100°	2040	2106	2236	2052	1537	2051
Case 4	-100°	70°	2.2E-4	4	7753	3679	4729	3428

4 Results and discussion

4.1 Effect of spray cone angle

In order to explore the effect of injection cone angle, the injection cone angle swing calculations (70° ∼ 150°) were carried out for the cases with injection timings at -50° and -100° ATDC in the engine idle condition. Figure 5 shows the variation of droplet and Equivalence Ratio (ER) distributions with injection angles for the late injection cases (SOI at -50° ATDC). With the wide injection angle (150°) as shown in Figure 5(a), droplets penetrate towards the corner between the liner and piston top surface and hit the cylinder liner. As indicated in Figure 6, approximately 13% of the total injected fuel stays in the wall film and crevice area in the late compression stroke. As the injection angle narrows, the fuel impingement area moves from the piston top and squish region to the piston bowl. The wall film fuel on the side wall of the piston bowl was predicted to be 11% in the 100° injection angle case, as compared to 20% of wall film fuel on the bottom part of the piston bowl with the narrow injection angle (70°).

Figure 7 and Figure 8 show the fuel, temperature, CO and uHC distributions with the wide and 100° injection angles at -5° ATDC, respectively. It should be noted that the conventional definition of equivalence ratio is used, and the ER distribution plots are calculated without accounting for kinetics. In the case of the wide injection angle, large amounts of the spray droplets move to the squish region as shown in Figure 5(a). As piston moves upwards, some droplets are trapped in the crevice area as observed in Figure 7(a), while most of them are pushed into the piston bowl. It can be seen that the fuel trapped in the crevice area contributes to the highest CO and uHC formations, due to the partial oxidation of fuel in the temperature range of 1300 ∼ 1400 K and the fuel rich condition. On the contrary, no trace of CO and uHC formation can be found in the crevice area with the 100° injection angle, where most of the fuel is injected into the piston bowl. Higher CO and uHC are found to be near the outer corner of the piston bottom and the centre part of the piston bowl. CO emission is determined primarily by the local equivalence ratio and temperature. As shown in Figure 8, the lean–fuel mixture mainly contributes to high CO at temperature below 1400 K at the centre of the piston bowl, while the rich-fuel burning at the temperature above 1800 K also produces high CO at the outer corner
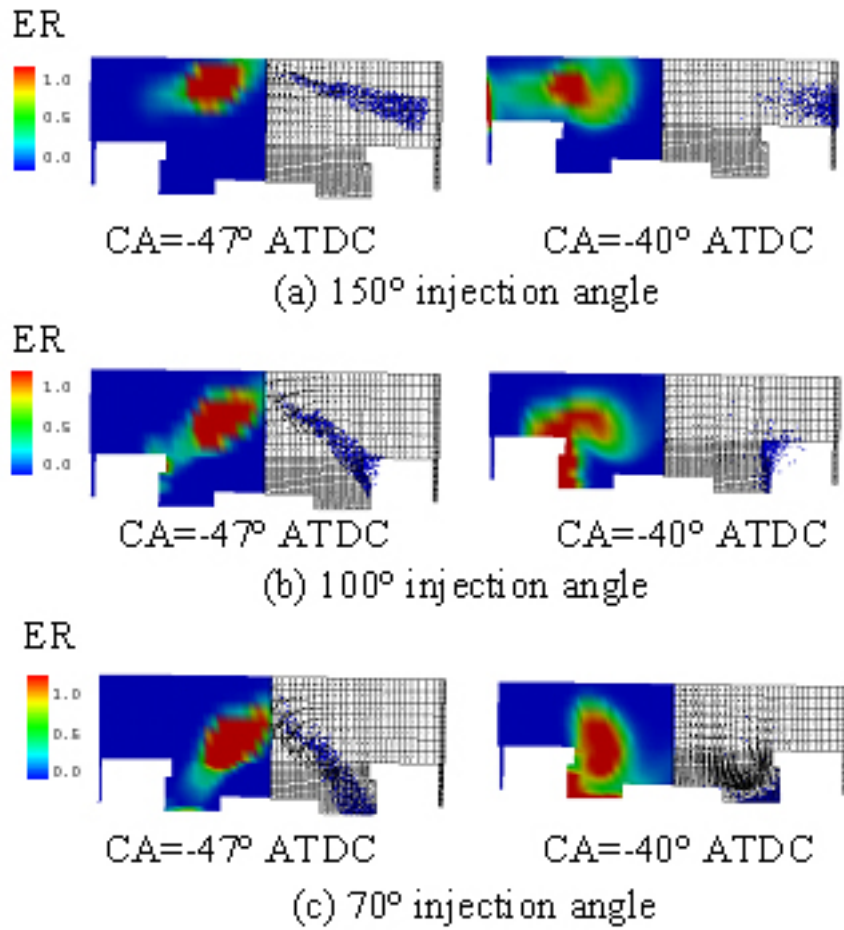
Figure 5: *Equivalence ratio (ER, left half plane) and droplet distribution (right half plane) of different injection angle with SOI at -50° ATDC.*
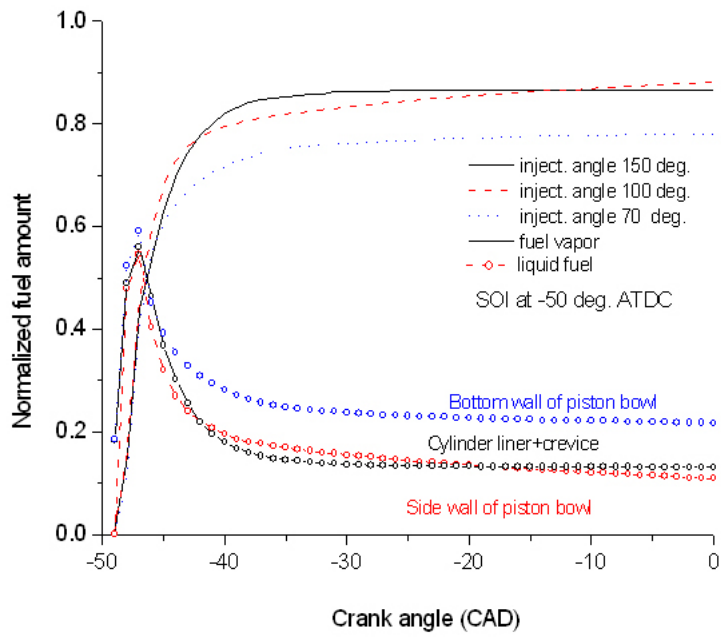
Figure 6: *Noralized fuel vapour and liquid fuel for different injection angle cases.*
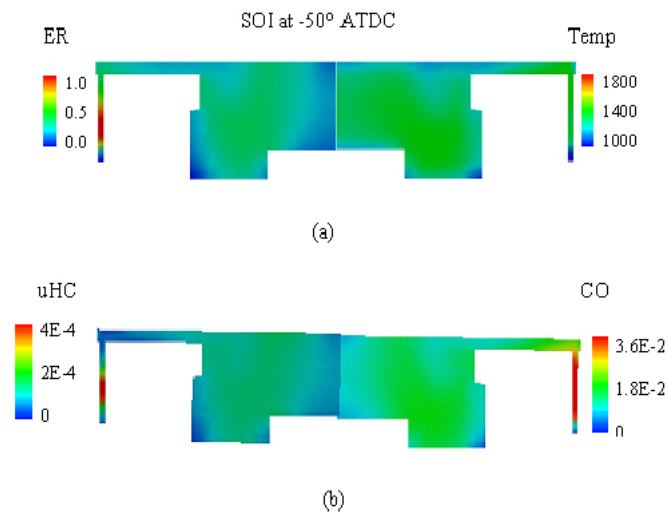
Figure 7: *Equivalence ratio, temperature, emissions distributions for 150° injection angle at -5° ATDC.*
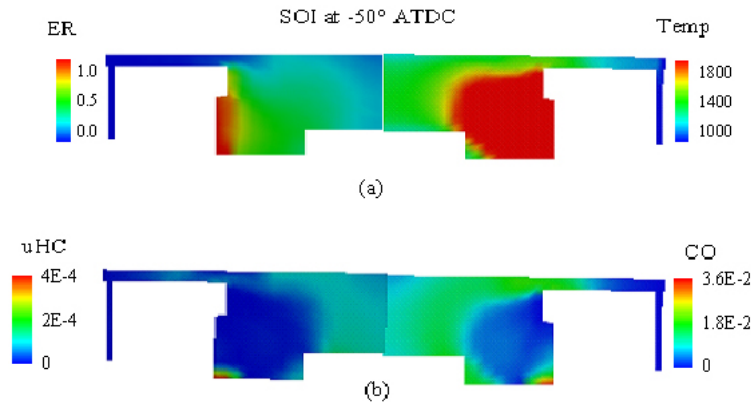
Figure 8: *Equivalence ratio, temperature, emissions distributions for 100° injection angle at -5° ATDC.*

of piston bottom in the absence of oxygen. Figure 10 shows the variation of pressure with injection angle at -50° ATDC injection timing. In the 100° injection angle case, the spray targets the corner of the piston bowl and splits the fuel into the piston bowl and the squish regions optimally. The peak pressure is the highest due to the minimum fuel wall film. If the injection angle is increased to 150° , as compared with the narrower injection angles, greater fuel loss and the partial oxidation of the trapped fuel in the crevice area with relative low temperature tends to incomplete combustion, and hence the lowest peak pressure and the highest uHC and CO emissions as shown in Figure 11.

Advancing the injection timing causes direct spray impingement on the cylinder wall as shown in Figure 11, regardless of the injection angle. Although the airflows induced by the spray and squish flow affect the mixing of the fuel and air, the distribution of liquid droplets and wall film fuel still dominantly influence the local mixture conditions. The fuel–rich mixtures are always found in the squish and crevice areas at all injection timings. Figure 12 shows the percentage of fuel impinged on the cylinder wall. At the low ambient gas density in the early injection case as shown in Figure 12, about 25% of wall film fuel was predicted by using the conventional CIDI wide angle injector. The excessive wall impingement results in larger fuel loss and deteriorates the mixture preparation, which leads to lower combustion efficiency and lower peak pressure as indicated in Figure 13. The wall impingement effect decreases as the injection angle narrows. With the narrower injection angle, the fuel impinges on the cylinder wall with a larger approach angle and the wall film spreads and splashes more widely. In contrast to the wide injection angle shown in Figure 12, most of wall film fuel evaporates at the later stage of the compression stroke and stays near the cylinder wall area in the two narrow injection angle cases. Only a slight pressure difference is seen in the two narrow injection angle cases as shown in Figure 13, due to the similar wall impingement characteristics and fuel distributions.

16
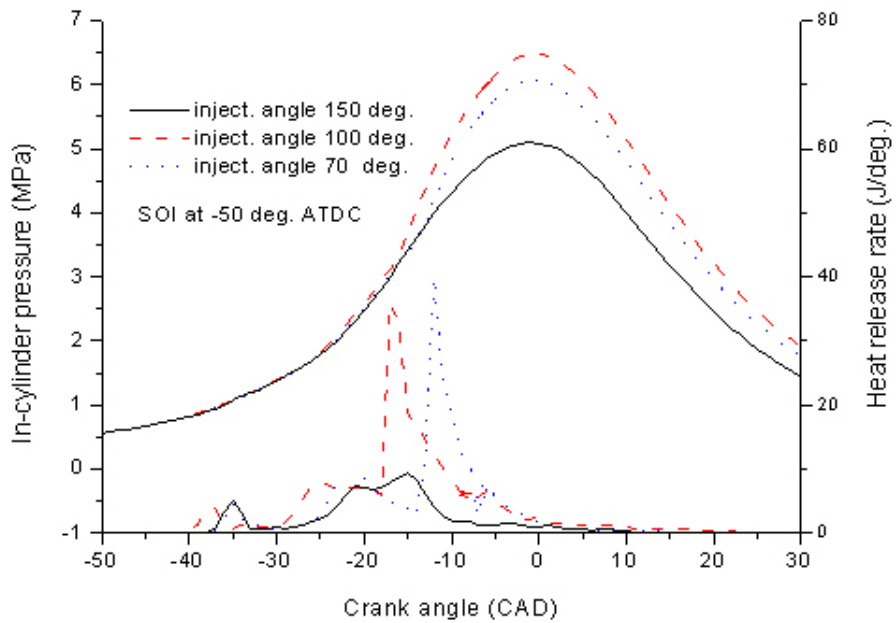
Figure 9: *The variation of pressure profiles with injection angle at -50° ATDC injection timing.*
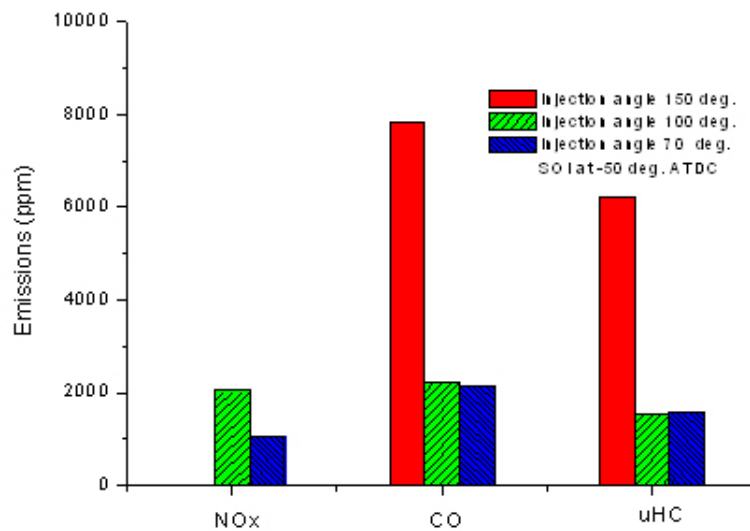
Figure 10: *The variation of emissions with injection angle at -50° ATDC injection timing.*
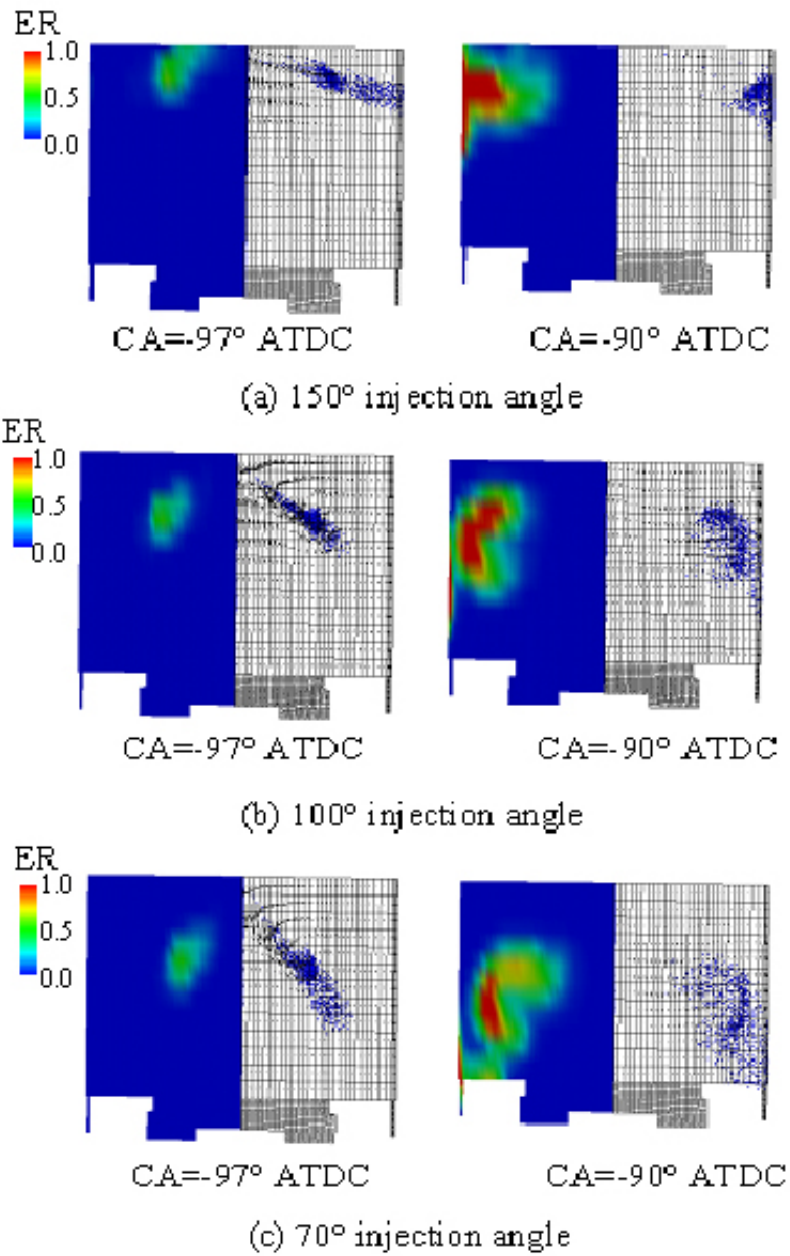
Figure 11: *Equivalence ratio (left half plane) and droplet distributions (right half plane) of different injection angle cases with SOI at -100° ATDC.*
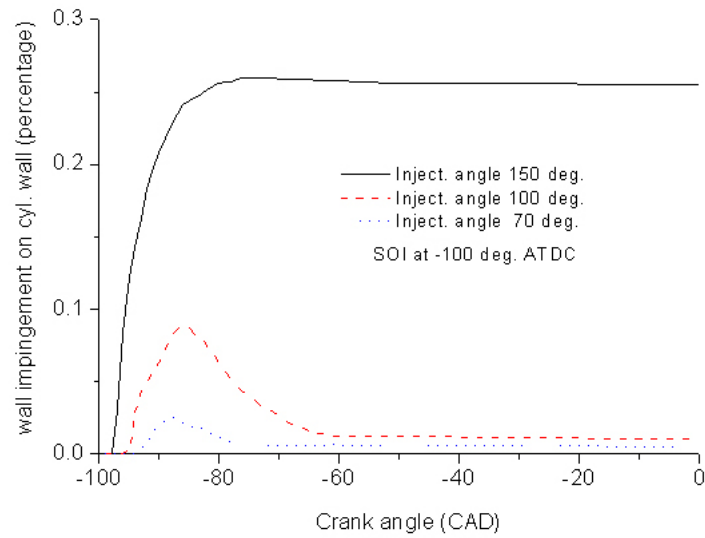
Figure 12: *The percentage of wall impingement on the cylinder wall at -100° injection timing.*

To understand the emissions results at the early injection timing, the detailed comparison between the 150° and 100° injection angles cases is presented in terms of fuel, temperature and emission distributions at -5° ATDC in Figure 14 and Figure 15. More fuel vapor is seen to be confined in the squish and crevice areas with the wide injection angle than with the narrow injection angle. This indicates that more fuel partial oxidations take place in the relatively low temperature area in the squish region, which contributes to higher CO emission in the wide injection angle case.

Table 4: *Combustion efficiency and emissions with different injection timings*

Start of injection (ATDC)	Combustion efficiency	NO$_x$ (ppm)	CO (ppm)	uHC (ppm)
-200°	35%	4.0E-4	8190.0	10253.0
-100°	38%	1.3E-4	9500.0	8269.0
-50°	83%	2040.0	2236.0	1537.0

19
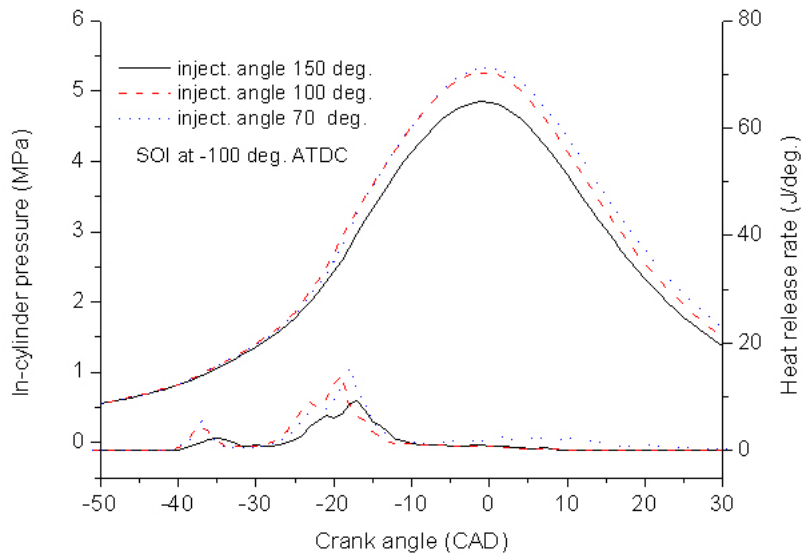
Figure 13: *The variation of pressure profiles with injection angle at -100° ATDC injection timing.*

(a)

(b)
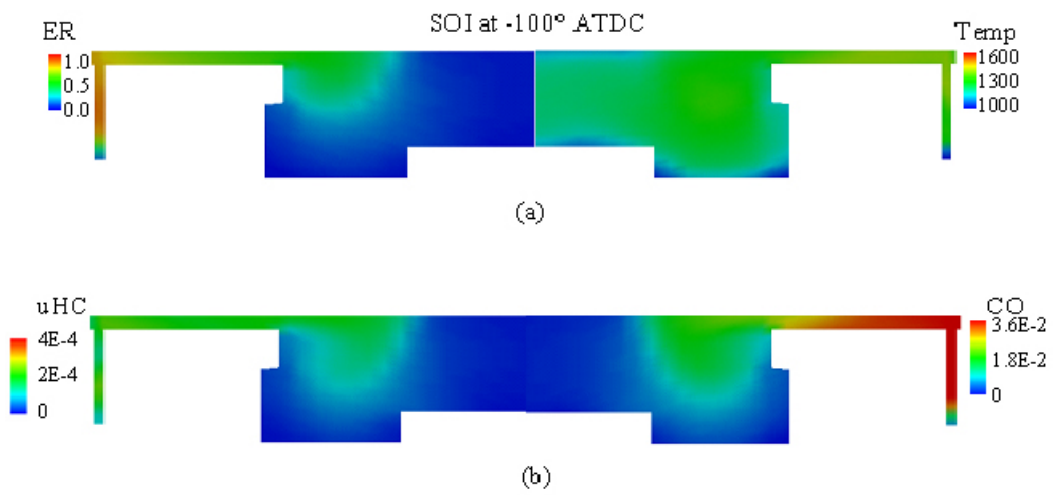
Figure 14: *Equivalence ratio, temperature and emissions distributions for 150° injection angle at -5° ATDC .*
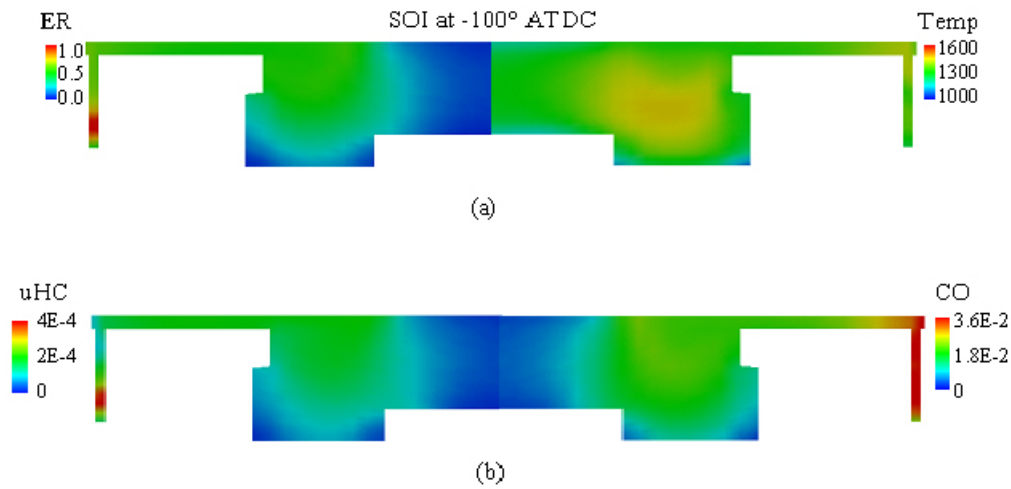
Figure 15: *Equivalence ratio, temperature and emissions distributions for 100° injection angle at -5° ATDC .*

4.2 Effect of injection timing

At late injection timing, the 100° injection angle was shown to enhance the mixing of air and fuel, due to the optimal droplet splash behavior at the edge of the piston corner. Hence, the simulation with this injection angle was considered to evaluate of the effect of injection timing. As shown in Figure 16, higher combustion efficiency indicated in Table 4 and higher peak pressure are seen with the retarded injection timing. This can be explained by referring to Figure 8(a) and Figure 15(a). The fuel stratification increases with the delayed injection, due to the limited time for mixing. More fuel–rich mixture is seen in the piston bowl region with relatively high temperature at the injection timing of -50° ATDC, contributing to more complete combustion and dramatically reduced CO and uHC emissions. If the injection timing is advanced earlier than -100° ATDC, the injection timing is shown to have little effect on combustion efficiency and peak pressure, but slightly increases uHC emissions. Obtaining the optimal mixture distribution in the combustion chamber is critical to improving the engine performance and lowering the CO and uHC emissions, especially in the engine idle condition. The multiple injections with the favorable injection timing and split ratio have the potential to avoid excessive wall wetting and optimize mixture distribution.
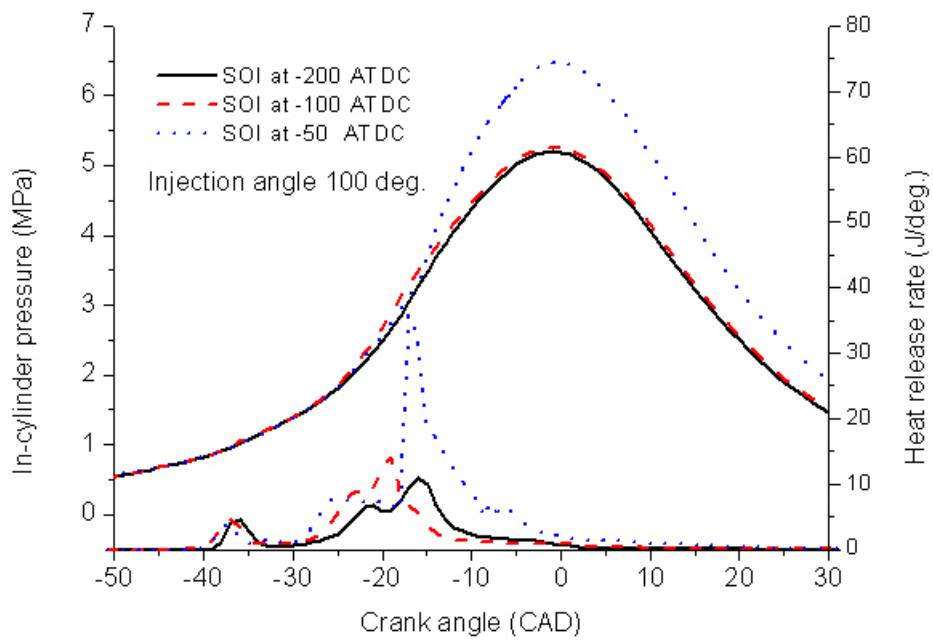
Figure 16: *The variation of pressure profiles with injection timing in the 100° injection angle cases.*

4.3 CFD–SRM correlation

A CFD simulation with detailed chemical kinetics can provide useful spatial information related to the distributions of fuel and temperature at the expense of high computational cost. In contrast, a zero–dimensional PDF based Stochastic Reactor Model (SRM) has its inherent advantages in terms of detailed chemical kinetics and the ability to account for inhomogeneities at low computational cost. However, in the SRM approach, the detailed flow description is approximated. Consequently, some empirical model constants in the simplistic spray model [15] and mixing model need to be calibrated, when the injection parameters (injection timing and injection angle) vary. In order to gain insight into the information with regard to the mixing time and fuel distribution, another objective of this study is to integrate CFD with the SRM, so as to develop a system level simulation tool capable of providing sufficiently reliable prediction of combustion parameters, such as pressure, temperature and emissions, within a reasonable computational time.

As demonstrated in the CFD simulation, with the early injection at -200° ATDC, it can be observed that there are three distinct physical zones, namely the bowl, squish and crevice regions, with different levels of stratification as shown in Figure 17. Initially most of the injected fuel stays in the squish region, due to the early injection. As the piston moves upwards, an appreciable amount of fuel is trapped in the crevice region, as indicated by the relatively fuel rich regions with low temperatures in Figure 17(b). At the end of the compression stroke, some part of the fuel in the squish region is pushed into the piston bowl by the increasing squish flow. (Note that the fuel in the piston bowl is leaner and with higher temperature than the other two regions). In order to take the characteristics into account, a multi–zone SRM approach is used in the early direct injection study. In this approach, the combustion chamber is split into the bowl, squish and crevice zones. The notional particle exchange between either the bowl and squish zones or the squish and crevice zones is considered based on the mass exchange due to pressure difference between the two neighbouring zones. Turbulent mixing time, indicated by the turbulent integral timescale τ as the volume averaged $\frac{\kappa}{\varepsilon}$, is neglected in the crevice zone, owing to the low crevice flow. While the mixing times in the bowl and squish regions are the inputs for the EMST mixing model. In this paper, this coupling is one–way, that is to say, the temporal evolution curves of mixing time in different zones as shown in Figure 18 are sampled at every computational timestep and used in the SRM code. The mixing time was obtained from CFD results based on the same engine.

It should be noted that the notional particles governed by the PDF evolution in the SRM model always correspond to certain fluid parcels in physical space. In order to make statistical comparisons between CFD and the SRM, the scatter plot of equivalence ratio v.s. temperature of all notional particles or computational cells is shown in Figure 19. It should be noted that the same initial conditions and engine parameters are applied to both the SRM and CFD codes. In the SRM, the model constant α, defined by the percentage of mass charge receiving liquid fuel over the total mass, needs to be calibrated. In the present study, α was set to 0.2 and the number of stochastic particles was chosen as 200. It can
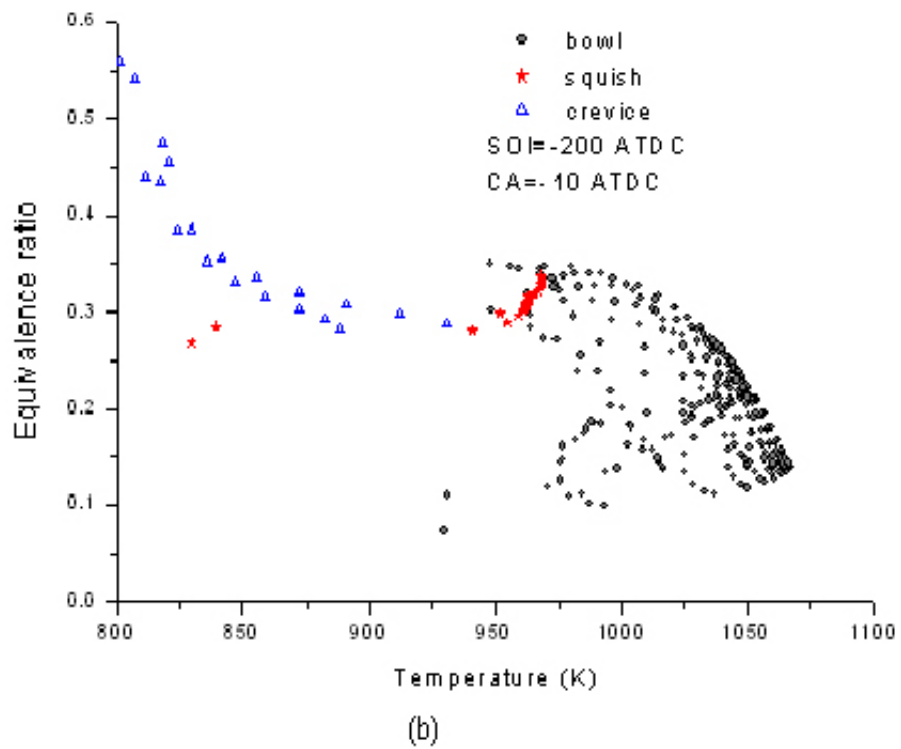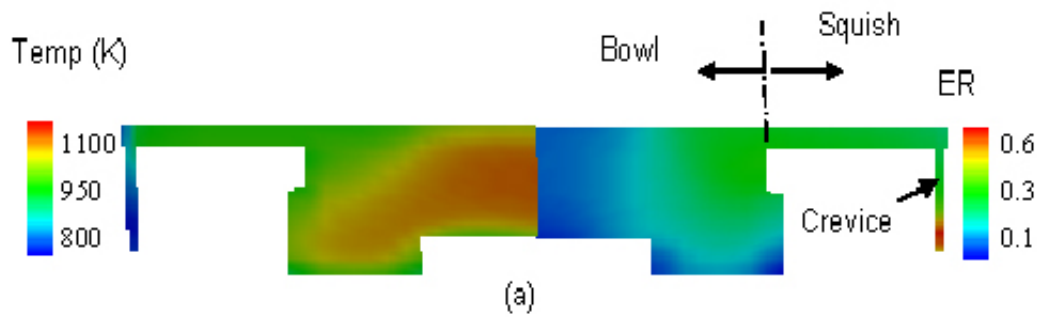
Figure 17: *The spatial distribution and scatter plot of temperature and equivalence ratio at 10° BTDC in pure mixing condition (without chemical reactions).*
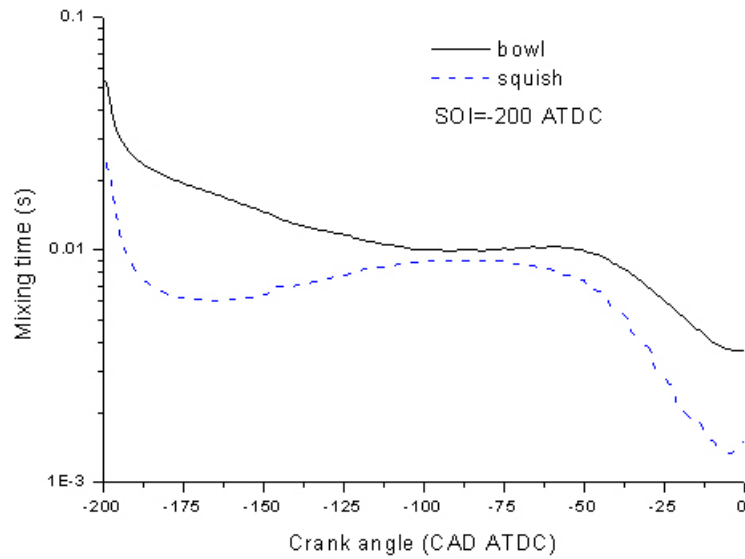
Figure 18: *The evolution of the volume–averaged mixing time in different zones with the early injection at -200° ATDC.*

be seen from Figure 19 that these two statistics plots obtained from CFD and the SRM correlate reasonably well in terms of the variance of equivalence ratio, especially in the bowl region. The variation trend of equivalence ratio and temperature are quite similar: as the piston approaches TDC, the variance in composition becomes smaller in the bowl and squish regions, due to the enhanced mixing by the squish flow. On the contrary, more heat losses contribute to larger thermal variation in the later compression stroke. As compared to the CFD results, the thermal variation is under–predicted by the SRM in the bowl and squish regions. This is due partly to the inherent limitation of Woschni's heat transfer model used in the study of HCCI combustion. In addition, there is a noticeable difference between the statistics plots in the crevice region. The discrepancy is possibly attributed to the lack of turbulent mixing assumed in the crevice zone in the multi–zone SRM approach.

Figure 20 shows the pressure profiles predicted by CFD, single–zone and multi–zone SRMs. It should be noted that the same initial conditions and model constants were used in both single–zone and multi–zone SRMs. As shown in Figure 20, the lowest peak pressure and earliest auto–ignition are predicted by CFD, due to the strongest thermal stratification and longer combustion duration as indicated in Figure 19. Comparing the single–zone and multi–zone SRMs, a more homogeneous mixture would be expected in the single–zone model, which results in a higher peak pressure as shown in Figure 20.

25
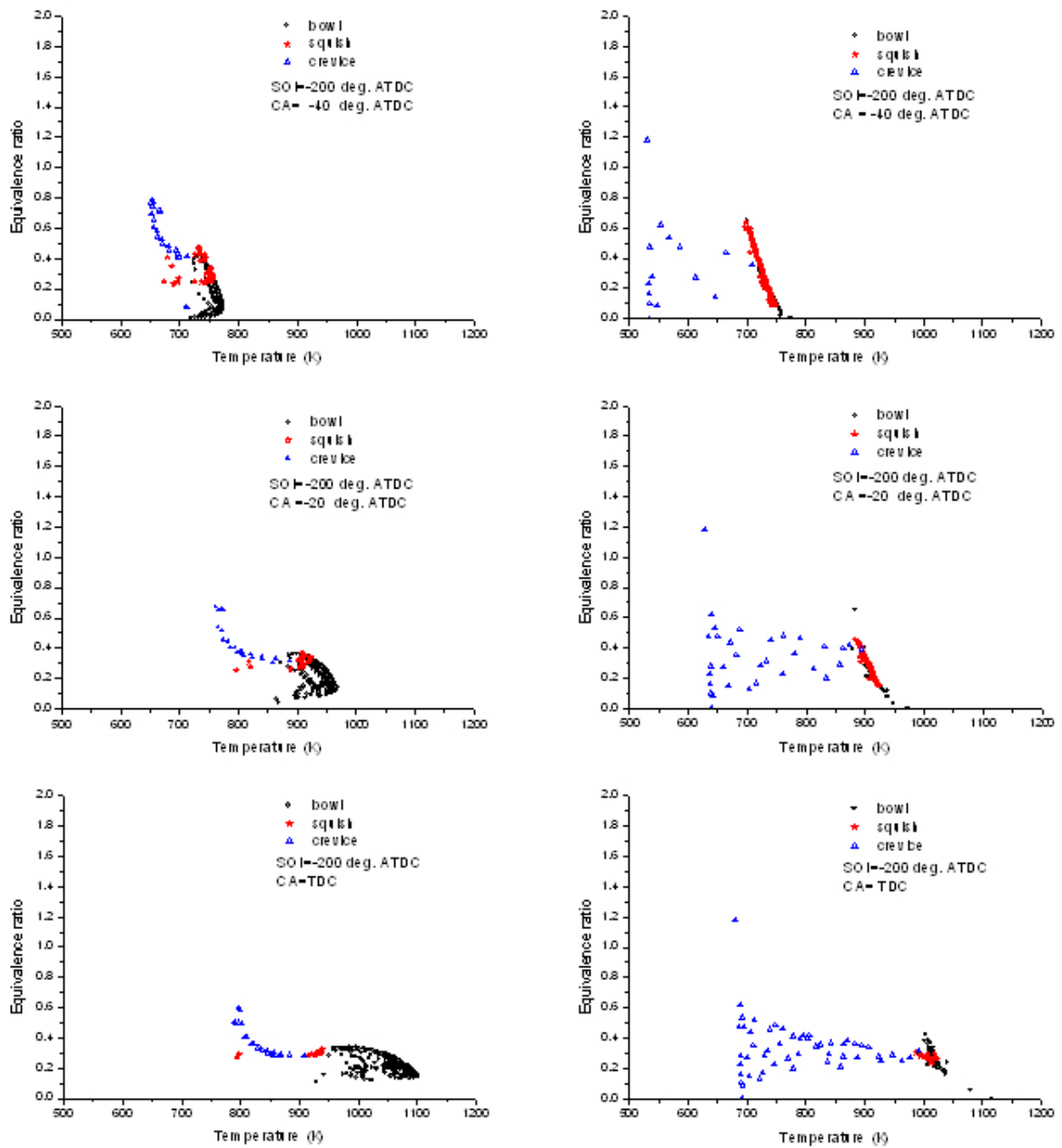
(a) computational cells in CFD   (b) notional particles in SRM

Figure 19: *The time evolution of scatter plots of CFD and SRM under the pure mixing condition (without reactions).*
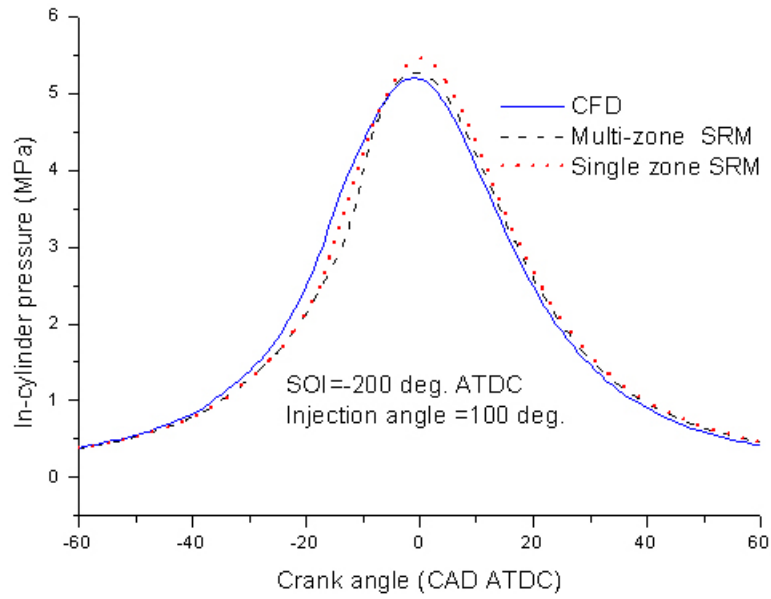
Figure 20: *Pressure profiles predicted by CFD, single–zone and multi–zone SRMs with SOI at -200° ATDC and 100° injection angle.*

As compared with the measured CO and uHC emissions, the predicted emissions from the multi–zone SRM coupled with CFD is seen to be higher than the simulation using the single–zone SRM, which correlates well with the measured value indicated in Table 5. Compared with the kinetics–coupled CFD simulation, the multi–zone SRM (with 200 notional particles) can reduce the CPU time by an order of magnitude as indicated in Table 5. The multi–zone SRM has shown the potential ability to predict emissions and pressure sufficiently well at lower computational cost, as compared to CFD. The further interactive integration of CFD with the SRM will be investigated in future work.

Table 5: *The predicted CO and uHC emissions and CPU time by CFD, single and multi-zone SRMs.*

	CO (ppm)	uHC (ppm)	CPU time (h)
Experiment	3268	4153	
CFD	7043	6157	22
Multi–zone SRM	2300	4290	2
single–zone SRM	1500	1840	2

5 Summary

Chemical kinetics integrated with two dimensional CFD was applied to study the effect of spray cone angle and injection timing on combustion characteristics and emissions in the engine idle condition. The conclusions can be summarized as follows:

The qualitative comparison of spray penetration indicates that the current hybrid KH–RT breakup model captures the transient spray behavior in low gas density condition reasonably well. The predicted pressure and emissions of NO_x, CO and uHC were seen to agree well with the measured values. The CFD–chemical kinetics model is capable of reproducing the ignition delay, main apparent heat release rate and the peak pressure.

As the injection is retarded to -50° ATDC, the spray impingement at the edge of the piston corner with 100° injection angle was shown to enhance the mixing of air and fuel, due to the optimal splitting of fuel droplets into the piston bowl and squish regions. The minimum fuel loss and more widely distributed fuel vapor contribute to the highest peak pressure and lowest uHC and CO emissions.

With the increase in the spray angle, the greater fuel loss and partial fuel oxidation in the crevice and squish regions tend to lower the peak pressure and increase uHC and CO emissions. Excessive wall wetting should be avoided in engine idle condition.

As the injection is retarded, the fuel stratification effect contributes to higher combustion efficiency and lower CO and uHC emissions. But with injection timing advanced earlier than -100° ATDC, the injection timing was shown to have little impact on combustion and peak pressure, due to the dominant effect of cylinder wall wetting.

The information of fuel distribution and mixing time was used in the multi–zone SRM. As compared to the single–zone SRM, the prediction of CO and uHC emissions was improved in the early injection PCCI combustion study. Further interactive coupling of CFD and the SRM will enable cycle to cycle simulation at low computational costs, while maintaining sufficiently reliable emissions predictions.

6 Acknowledgments

References

[1] S. Aceves and D. L. Flowers. A Multi-zone Model for Prediction of HCCI Combustion and Emissions. SAE paper 2000-01-0372, 2000.

[2] A. Amsden. KIVA–3V: A Blocked-structured KIVA Program for Engine with Vertical or Canted Valves. LA-13313-MS, 1997.

[3] A. Babajimopoulos, G. Lavoie, and D. N. Assanis. Modelling HCCI Combustion with High Levels of Residual Gas Fraction-A Comparison of two VVA Strategies. SAE paper 2003-01-3220, 2003.

[4] M. Christensen, H. A., and B. Johansson. Demonstrating the Multi Fuel Capability of a Homogeneous Charge Compression Ignition Engine with Variable Compression Ratio. SAE Paper 1999-01-0367, 1999.

[5] D. Flowers, S. Aceves, R. Martinez, R. Hessel, and R. W. Dibble. Effect of Mixing on Hydrocarbon and Carbon Monoxide Emissions Prediction for Isooctane HCCI Engine Combustion using A Multi-zone Detailed Kinetics Solver. SAE paper 2003-01-1821, 2003.

[6] A. Gray and T. W. Ryan III. Homogeneous Charge Compression Ignition of Diesel Fuel. SAE paper 971676, 1997.

[7] Z. Han and R. Reitz. A Temperature Wall Function Formulation for Variable-Density Turbulent Flows with Application to Engine Convective Heat Transfer Modelling. *International Journal of Heat and Mass Transfer*, 40:40–60, 1997.

[8] A. K. Hayashi, T. Miyamoto, A. Harada, S. Sasaki, H. Akagawa, and K. Tsujimura. Approaches to Solve Problems for the Premixed Lean Diesel Combustion. SAE paper 1999-01-0183, 1999.

[9] J. B. Heywood. *Internal Combustion Engine Fundamentals*. McGraw-Hill, New York, 1988.

[10] K. Inagaki, T. Fuyuto, K. Nishikawa, K. Nakakita, and I. Sakata. Duel-fuel PCI Combustion Controlled by In-cylinder Stratification of Ignitability. SAE paper 2006-01-0028, 2006.

[11] S. Kimura, O. Aoki, Y. Kitahara, and E. Aiyoshizawa. New Combustion Concept for Ultra-clean and High-efficiency Small DI Diesel Engine. SAE paper 1999-01-3681, 1999.

[12] S. Kong and R. Reitz. Application of Detailed Chemistry and CFD for Predicting Direct Injection HCCI Engine Combustion and Emissions. *Proceedings of the Combustion Institute*, 29:667–669, 2002.

[13] S. Kook and C. Bae. Combustion Control Using Two-stage Diesel Fuel Injection in a Single-cylinder PCCI Engine. SAE paper 2004-01-0938, 2004.

[14] M. Kraft, P. Maigaard, F. Mauss, M. Christensen, and B. Johansson. Investigation of Combustion Emissions in a Homogeneous Charge Compression Ignition Engine: Measurements and New Computational Model. *Proceedings of the Combustion Institute*, 28:1195–1201, 2000.

[15] S. Mosbach, H. Su, M. Kraft, A. Bhave, Z. Wang, and J. Wang. Dual Injection HCCI Engine Simulation using a Stochastic Reactor Model. *International Journal of Engine Research*, 8:41–50, 2007.

[16] G. Neely, S. Sasaki, Y. Huang, J. Leet, and D. Stewart. Diesel Emission Control Strategy to Meet US Tier 2 Emission Regulations. SAE paper 2005-01-1091, 2005.

[17] P. O'Rourke and A. A. Amsden. A Spray/Wall Interaction Submodel for the KIVA-3 Wall Film Model. SAE paper 2000-01-0271, 2000.

[18] M. A. Patterson and R. Reitz. Modelling the Effect of Fuel Spray Characteristics on Diesel Engine Combustion and Emissions. SAE 980131, 1998.

[19] Y. Ra and R. Reitz. The Use of Variable Geometry Sprays with Low Pressure Injection for Optimization of Diesel HCCI Engine Combustion. SAE paper 2005-01-0148, 2005.

[20] H. Su, S. Mosbach, M. Kraft, A. Bhave, S. Kook, and C. Bae. Two-stage Fuel Direct Injection in a Diesel Fuelled HCCI Engine. SAE paper 2007-01-1880, 2007.

[21] D. Tamagna, Y. Ra, and R. Reitz. Multi-dimensional Simulation of PCCI Combustion Using Gasoline and Duel-Fuel Direct Injection with Detailed Chemical Kinetics. SAE paper 2007-01-0190, 2007.

[22] Y. Z. Zhang, E. Kung, and D. Haworth. A PDF Method for Multi-dimensional Modelling of HCCI Engine Combustion: Effects of Turbulence/Chemistry Interactions on Ignition Timing and Emissions. *Proceedings of the Combustion Institute*, 30: 2763–2771, 2005.